Chapter 11
Delayed Fracture After Long Exposure in Atmospheric Environments

11.1 Background

Delayed fracture of newly developed high-strength steel bolts in highway constructions in the mid-1960s was a severe alert to the civil engineering community and the Japanese steel industry aiming for higher-strength steel. It triggered extensive studies on the mechanism and effective means to prevent failure, but an upper limit to the strength level is still imposed in the use of high-strength steel bolts [1]. The increased susceptibility to delayed fracture in service with higher-strength steel is still a potential and crucial issue in recently developing weight-reducing steel components in vehicles and hydrogen-energy equipment.

Delayed fracture of steel is described in Sect. 6.4. A major difficulty in establishing viable principles for steel design and a reliable assessment of the performance is the lack of laboratory test methods to simulate long-term atmospheric exposure. Environmental conditions are diverse in sites and time, and the use of steel components extends over many years. An inevitable acceleration in laboratory tests might alter the actual situation for crack initiation and propagation. Little published information about the failure in service has retarded revealing the entity of failure. Attention has been paid conventionally to the amount of hydrogen entering from environments as the primary cause of delayed fracture. Still, in technical aspects, even its quantitative analysis was limited in the early days.

Recent progress in experimental and theoretical tools is remarkable, such as hydrogen thermal desorption analysis, hydrogen visualization, microstructural and fractographic observations, and computational science. Intensive studies have almost elucidated characteristic features of hydrogen embrittlement (HE) in general, and proposed models of the mechanism of HE may have covered feasible aspects of understanding the function of hydrogen, as described in the preceding chapters. However, tailored laboratory experiments and computations remain to justify the validity of their results in engineering practice.

M. Nagumo, *Fundamentals of Hydrogen Embrittlement*,
https://doi.org/10.1007/978-981-99-0992-6_11

11.2 Peculiar Situations of Delayed Fracture as Material Failure

(a) External driving force for fracture

Fracture is the process that a bulk material separates, creating new surfaces. To proceed with the process, the energy of the original bulk must be higher than the separated one that includes new surfaces, as shown in Fig. 11.1. The energy difference between the initial and the final states is the driving force of fracture, and its increase is necessary for a fracture to occur. Further, the energy transition must overcome the energy wall to activate the process. For the free surface formation by decohesion of atomic bonds, a high stress of the theoretical fracture strength, ~ $E/10$, must be present. On the other hand, in a plasticity-controlled fracture, flow stress is enough to drive the process.

In ordinary mechanical tests, raising the applied load increases the energy of the original body in the form of elastic and plastic energy. However, the stress state of a steel bolt in engineering service is usually under a constant load or displacement condition, except for variations due to environmental conditions, without an increase in the applied stress. An external supply of mechanical energy is not expected to increase the driving force. A small amount of hydrogen, of the order of ppm, entering from environments is not feasible to increase the internal energy of the steel to fracture.

On the other hand, the presence of impurity atoms lowers the surface energy, as illustrated in Fig. 9.4. A decrease in the surface energy due to hydrogen segregation was discussed by Petch [2] in Sect. 9.2 and Yamaguchi et al. [3] as an increasing driving force in intergranular (IG) fracture in Sect. 9.4.1. The surface energy effects before a crack formation are not definite as the driving force. However, hydrogen entering from environments is intuitively a stimulator of delayed fracture, putting aside its mechanism. Leaving behind the discussion about the function of hydrogen, laboratory tests of sustained-loading delayed fracture, up to 100 h or so at room temperature, demonstrated a decisive role of hydrogen concentrations in delayed fracture, leading to the concept of the critical hydrogen concentration as described in Sect. 6.4.4.

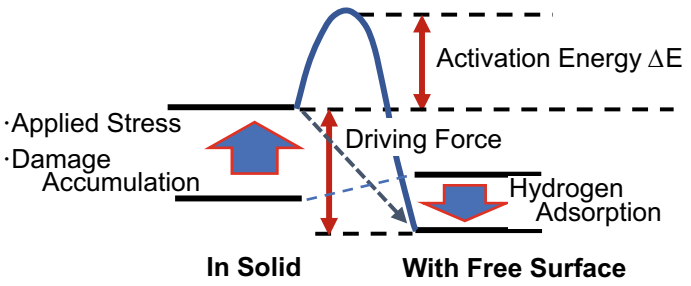

Fig. 11.1 Energy states for a fracture to occur

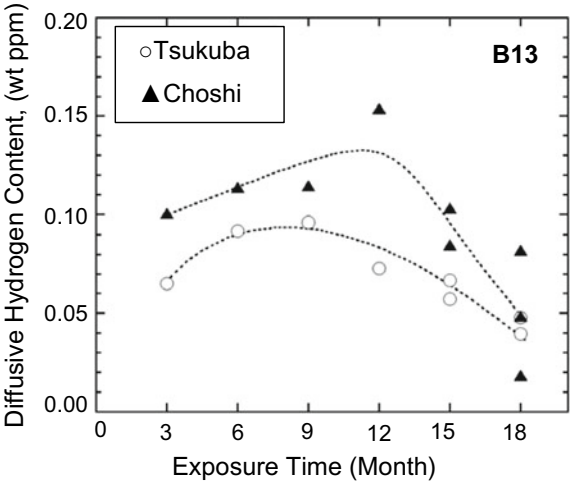

Fig. 11.2 Hydrogen contents in high-strength steel bolt exposed at two sites, Tsukuba (inland) and Choshi (coast side) in Japan (Li et al. [4])

A crucial fact is that a continuous increase in hydrogen contents has never been observed in high-strength steel specimens subjected to long-time atmospheric exposure. Hydrogen absorption during atmospheric exposure in U-shape bent 1500 MPa high-strength steel plates are shown in Fig. 6.33. Figure 11.2 shows hydrogen contents in high-strength steel exposed for up to 18 months at two sites, coast side and inland, in Japan [4]. The steel was AISI 4135 (0.36%C-Cr–Mo) of 1310 MPa in tensile strength, and the specimens were circumferentially notched bars of 10 mm diameter. The specimens were fastened and fixed to pored steel pipes with the applied stress of 1.1 and 0.9 of the tensile strength of a smooth bar. Similar to Fig. 6.33, the hydrogen content turned to decrease after an initial continuous increase. The fracture stress of the exposed specimens, measured with a slow strain-rate tensile test, was almost the same irrespective of the exposure time.

(b) Feasible factors in increasing driving force

The findings imply difficulty in applying laboratory simulation results straightly to delayed fracture in a long-time atmospheric exposure in so far as using the hydrogen concentration as a parameter. On the other hand, in atmospheric exposure, specimens tolerate various stimulations, besides the entry of hydrogen. As a process that steadily increases the driving force, suggestive findings are the effects of environmental variation in the delayed fracture in Sect. 6.4.3, and stress histories to accumulate damage in Sect. 7.4.2. Change in the internal stress fields by the entry of hydrogen is demonstrated in a stress-relaxation experiment shown in Fig. 5.5.

Microstructures of most high-strength steel bolts are tempered-martensite with substantially high dislocation densities. Dislocation configurations vary by thermal histories like tempering and are not entirely stable against external stimulations. During atmospheric exposure, the fastened bolts tolerate environmental variations of humidity and temperature, causing periodic hydrogen entry and variations of the

applied stress. A reasonable consequence is that such variations destabilize dislocation configurations. Observed accumulation of vacancy-type lattice defects likely results from the activated dislocations, promoting delayed fracture. The damage accumulation causing crystallinity deterioration increases the driving force for fracture, even without increasing hydrogen concentration and applied stress.

The above reductions, on a line of recently developed knowledge, though mostly in laboratory studies, give a way to understand the nature of delayed fracture in long-time atmospheric exposure. However, a crucial difficulty has been the lack of proper materials to be examined. In such a situation, acquiring, by chance, a high-strength steel bolt subjected to atmospheric exposure for 16 years and retrieved within 24 h after the fracture enabled the first detailed observation of the cracking process [5]. The following summarizes the main results.

11.3 Fractographic Features and Microscopic Process of Cracking

11.3.1 Material

The steel was a medium-carbon Cr–Mo steel, SCM435 in the Japanese Industrial Standard (JIS), similar to AISI 4135. The microstructures are acicular martensite prepared by oil quenching from 1133 K and subsequent tempering at 733 K for 110 min and followed by water quenching. Mechanical properties are shown in Table 11.1. The screw-threaded bolt was a JIS hexagon head bolt of 22 mm diameter and 85 mm shank length. It was fastened to a steel plate through a hole with a nut and two washers to the axial force of 346 kN.

Loading of the bolt was under a constant-displacement mode. The axial force for fastening exceeded the elastic limit, and the stress concentration at the screw groove enhanced plastic deformation in the region close to the groove root. The maximum principal stress and equivalent plastic strain distributions along the screw-threaded shank were approximately expressed in Fig. 11.3 [5] for circumferentially V-notched round bar specimens of 0.25 mm in root radius, calculated using a finite element method. The exposure was at a coast side in Okinawa, Japan, and Fig. 11.4 shows the whole appearance of the failure bolt and its fastened state. Failure in the present case occurred at the second groove from the screw-groove start.

Table 11.1 Tensile properties of the steel

0.2 PS	UTS	El	RA
1202 MPa	1312 MPa	15.8%	53.4%

0.2 PS: 0.2% proof stress, UTS: ultimate tensile stress, El: elongation to fracture, RA: reduction of area

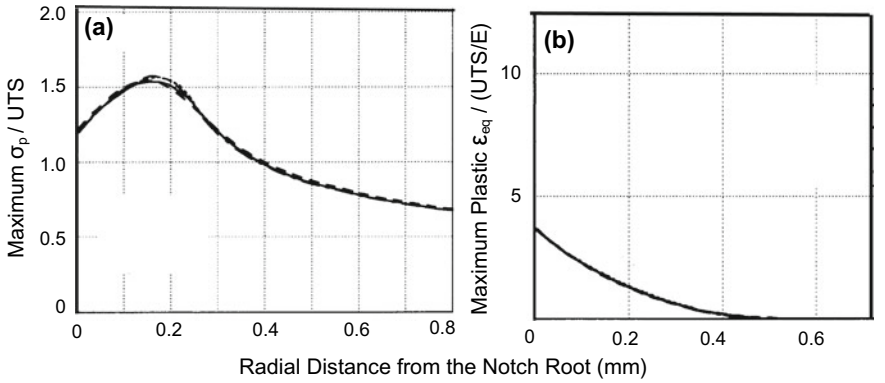

Fig. 11.3 Finite element method calculations of stress and plastic strain along the radial direction. **(a)** Maximum principal stress σ_p normalized by ultimate tensile stress. **(b)** Maximum equivalent plastic strain ε_{eq} normalized by elastic fracture strain (= ultimate tensile stress/Young's modulus E). The diameter of the bar was 10 mm, and the 60 V circumferential notch was 2 mm in depth with a root radius of 0.25 mm. Calculations were conducted for four high-strength steels of 1313, 1492, 1455, and 1772 MPa in UTS and 1202, 1304, 1345, and 1596 in 0.2% PS, respectively. Young's modulus and Poisson's ratio were commonly set at 205 GPa and 0.3, respectively [5, 13]

Fig. 11.4 **(a)** Whole view of the broken bolt. **(b)** Fastened state of bolts to steel plates

11.3.2 Entire Cracking Process

A rough image of the cracking process is apparent in Fig. 11.5 [5] of optical micrographs of pair fracture surfaces; the crack initiation is in a small area close to the outer surface on the left, followed by radial propagation. The broken bolt was retrieved within 24 h after the fracture, but small rust spots, though not very many over the entire fracture surface and too small to discern in the micrographs, were present in Fig. 11.5(a). Rust stain was explicit on the opposite side, Fig. 11.5(b). The presence of slight rusting suggests that the propagation of the initiated crack was not catastrophic and that roughly one week or so had passed after the crack initiation until the final separation. In Fig. 11.5, to be noticed is the crack initiation close to the outer surface. Figure 11.6(a) [5] is a magnified optical micrograph of the dark part on the

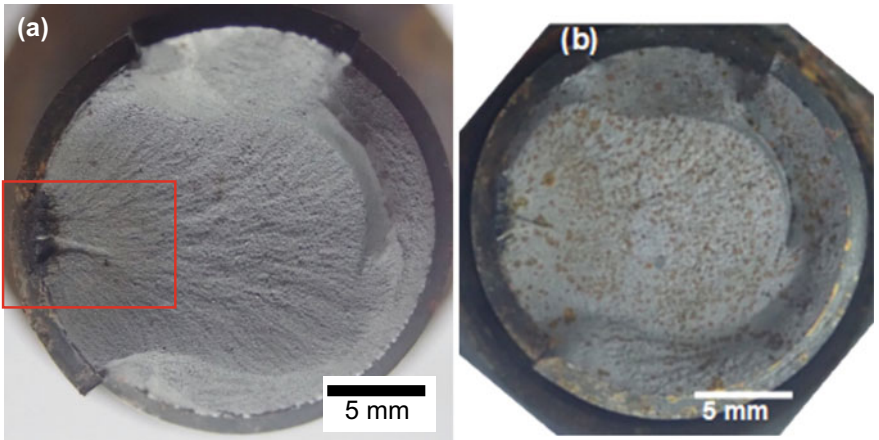

Fig. 11.5 **(a)** Optical micrograph of the entire fracture surface and **(b)** the pair fracture surface of (**a**) (Homma et al. [5])

left edge. The region is seemingly affected by heavy rusting, and small particles indicated by yellow arrows are likely rust spots. Figure 11.6(b) is a magnified secondary electron image of a scanning electron micrograph (SEM) of the red-framed area in Fig. 11.5(a). The different contrasts in Fig. 11.6(a) and (b) are likely because of each imaging principle. The contrast in the optical micrograph is due to the surface materials' reflectance, interference, and specimen inclination. On the other hand, the contrast in the SEM image is mainly due to the atomic number and roughness of the surface materials. Dark contrasts in Figs. 11.5(a) and 11.6(a) are likely due to thin surface materials and the surface inclination.

However, the SEM image in Fig. 11.6(b) of the dark area is relatively sharp, with no corrosion pits and substantial corrosion products. The thin dark area along the outer surface was the starting *area*, *not a point*, of striated crack propagations. Fan-like patterns in Fig. 11.6(b) characterize the crack propagation. As described in Sect. 11.3.4, fracture morphologies successively altered with the crack propagation, and the fan-like patterns in Fig. 11.6(b) correspond to the alteration of fracture morphologies. The fan-like patterns and a dark part in the middle of Fig. 11.6(b) are primarily due to the roughness and inclination of the fracture surface.

Stress corrosion cracking (SCC) was a candidate mechanism of delayed fracture in atmospheric exposure. However, no findings were present to support the notion in the present case.

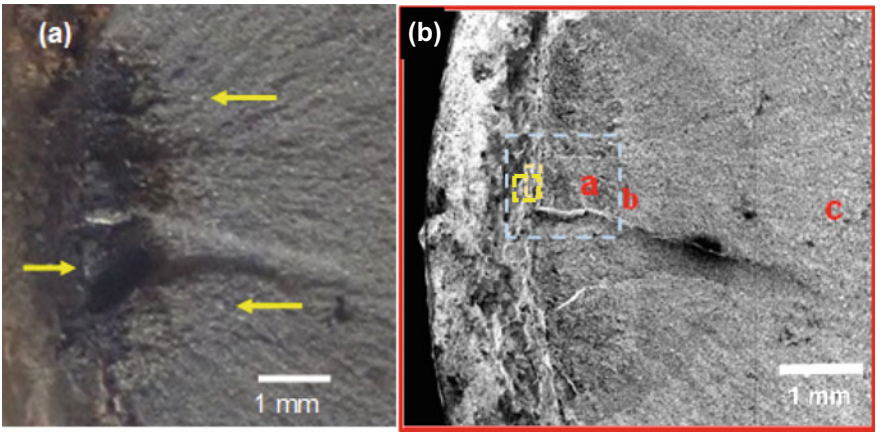

Fig. 11.6 **(a)** Magnified optical micrograph of the dark area in the left side of Fig. 11.5(a). Yellow arrows indicate small particles likely of rust spots. **(b)** SEM micrograph of an area near the crack initiation site indicated by the red frame in Fig. 11.5(a). The blue and yellow dashed frames indicate the areas in (**a**) and Fig. 11.9(a), respectively. Letters a, b, and c indicate the sites of areas (**a**), (**b**), and (**c**), respectively, in Fig. 11.13 (Homma et al. [5])

11.3.3 Crack Initiation Site—Frail Zone

11.3.3.1 Multiple Crack Nucleation and Their Mergence

In the zone from which the striated crack propagated, multiple cracks were present. Figure 11.7(a) [5] shows 3-dimensional SEM images, and broad dark lines, indicated by yellow arrows, are steps between neighboring crack surfaces on different planes. Details of Step 2 are in Fig. 11.7(b) by tilting the specimen by 60° around the horizontal axis (i.e., the crack growth direction). Arrow 3 indicates the opening between neighboring fracture surfaces, and two cracks on Surfaces I and II merge to form a planar crack, as circle 5 indicates. Multiple crack nucleation was also manifested as numerous small cracks on the outer surface of the bolt, as indicated by arrow 4 in Fig. 11.7(a). Intersections of small cracks with the outer surface are not the same, as Fig. 11.8 [5] shows shear for fracture surface I while a straight intersection for lower fracture surface II.

An issue about multiple crack nucleation is which stress or strain controls the crack nucleation. The stress and strain distributions under the screw groove are in Fig. 11.3. The fracture surface topography analysis (FRASTA), which detects the crack nucleation site and propagation process on a computer [6, 7], is useful for detecting the time sequence of multiple crack nucleation. Under an increasing load applied to a specimen, failure is to begin at some weak spots or stress concentrators in the form of a microcrack or microvoid. Three-dimensional images of mating fracture surfaces are first fully coalesced and then successively separated on the computer.

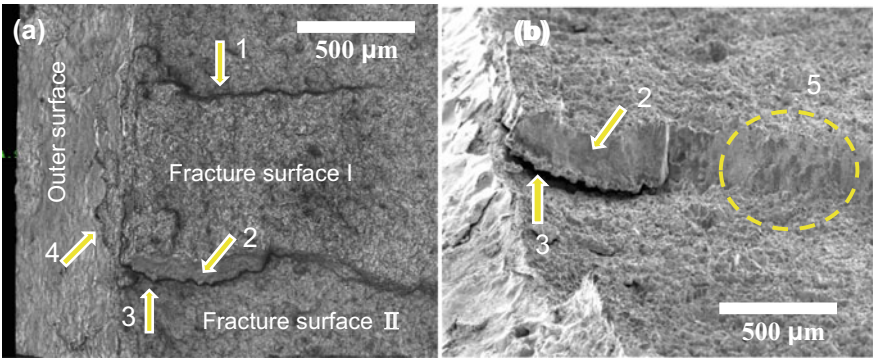

Fig. 11.7 SEM images of the crack initiation site. **(a)** Downward 3-dimensional image showing multiple cracks on the fracture surface; arrows 1 and 2 indicate steps between neighboring crack surfaces on different planes. Arrow 4 is a crack that developed on the outer surface of the bolt. **(b)** SEM image tilting the specimen by 60° around the horizontal axis (i.e., the crack growth direction) showing the details of an enlarged view of step 2. Arrow 3 indicates the opening between neighboring fracture surfaces, and circle 5 shows the mergence of two cracks on surfaces I and II (Homma et al. [5])

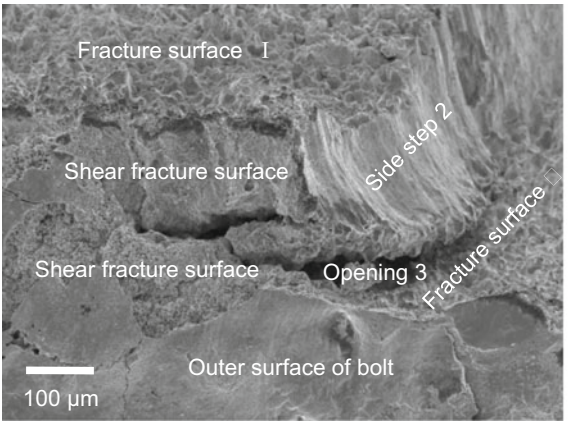

Fig. 11.8 SEM image of the intersection site of cracks with the outer surface of the bolt obtained by tilting the specimen in Fig. 11.6(b) by 60° around the horizontal axis. Side step 2 is the same as arrow 2 in Fig. 11.7. Fracture surface I reaches the outer surface forming shear fracture, whereas lower fracture surface II directly intersects the outer surface (Homma et al. [5])

The extension of the open area is recorded following the increase in the separation distance "s".

The FRASTA results in Fig. 11.9 [5] show successive separations, in green, of the mating fracture surfaces by a distance "s". Separation first appeared on fracture surface I at a site around 500 μm from the edge, as arrow *a* indicates, and the separation extended toward the edge. On the other hand, on fracture surface II,

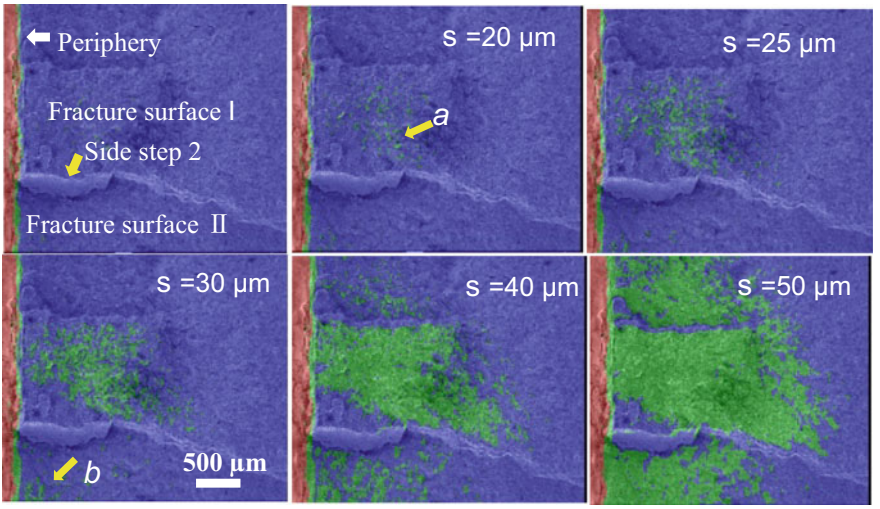

Fig. 11.9 FRASTA results for crack nucleation and propagation with increasing the separation distance between mating upper and lower fracture surfaces of the bolt. Separated parts are denoted in green. The separation distance is denoted by "s". Sites *a* and *b* are the first nucleation sites in each of the neighboring fracture surfaces (Homma et al. [5])

separation first appeared at a site very close to the edge, as arrow *b* indicates, and extended inward. The stress and strain states at the crack nucleation sites in Surface I and II are different, according to Fig. 11.3.

Multiple crack nucleation without forming a propagating crack was revealed beneath the outer surface of an unbroken part of the bolt. Figure 11.10 [5] is a SEM micrograph of a cross-section parallel to the tensile axis beneath the screw groove second-next to the fractured surface. The observed area (a) was about 200 μm from the groove root, showing multiple nucleation and branching of cracks along prior austenite grain boundaries. Insert (b) in Fig. 11.10 is a magnified view of the red-framed area in (a), showing the mating of irregularly shaped and flat crack surfaces and also a separately nucleated microcrack. It is similar to a microcrack observed by Shibata et al. in Fig. 7.8 [8]. The findings indicate that a thin zone a few hundred μm beneath the screw groove root, specifically along prior austenite grain boundaries, is frail and ready to form microcracks. The depth coincided with the zone of intensified stress and strain in Fig. 11.3. Since the final crack propagation likely took place in a short period, say one week or so, the long time of 16 years until the delayed fracture might be spent to deteriorate this zone ready to fracture. We conventionally use "*frail zone*" for this deteriorated zone, and using the term "*frail*" instead of "embrittled" was to evade the latter's implication of a specific type of fracture.

Figure 11.11 shows [5] the deduced process of crack nucleation in atmospheric exposure. The role of hydrogen in damage generation and accumulation is well understood with the HESIV mechanism, the hydrogen-enhanced strain-induced vacancies, described in Sect. 10.5. Direct observations of the nanoscopic process of crack

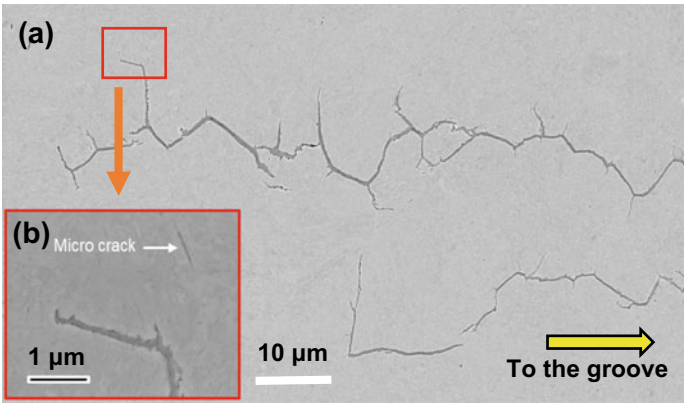

Fig. 11.10 **(a)** SEM micrograph showing multiple nucleation and branching of cracks in an area about 200 μm from the groove root next to the fractured one. The view is a cross-section parallel to the tensile axis. **(b)** is the magnified view of the red-framed area in (**a**), showing mating of irregularly shaped and flat crack surfaces and also a separately nucleated microcrack (Homma et al. [5])

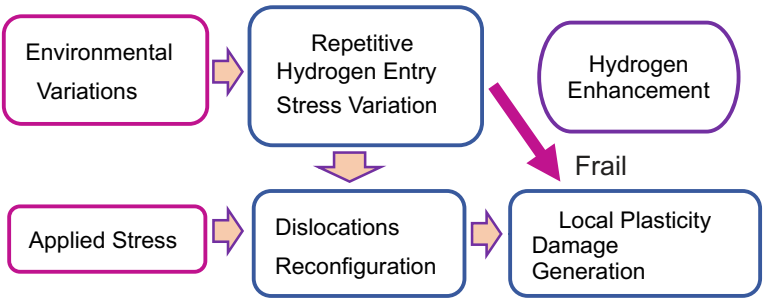

Fig. 11.11 The supposed process of damage accumulation under atmospheric exposure to form the frail zone (Homma et al. [5])

or void formation are lacking. Still, the molecular dynamics (MD) simulations on nanovoid formation in bi-crystal nickel [9] support the notion of damage accumulation leading to nanovoid formation. Hydrogen also prepares the crack propagation path, as described in Sect. 11.3.4.

11.3.3.2 Three-Dimensional Intergranular Fracture

The net-like cracking along prior austenite grain boundaries shown in Fig. 11.10 supports the idea that independently nucleated fine cracks link along grain boundaries in the frail zone. The net-like microcrack nucleation indicates that the orientation of grain boundaries does not control the crack nucleation, while the macroscopic crack extension is under the externally applied-stress control. Figure 11.10 shows a site

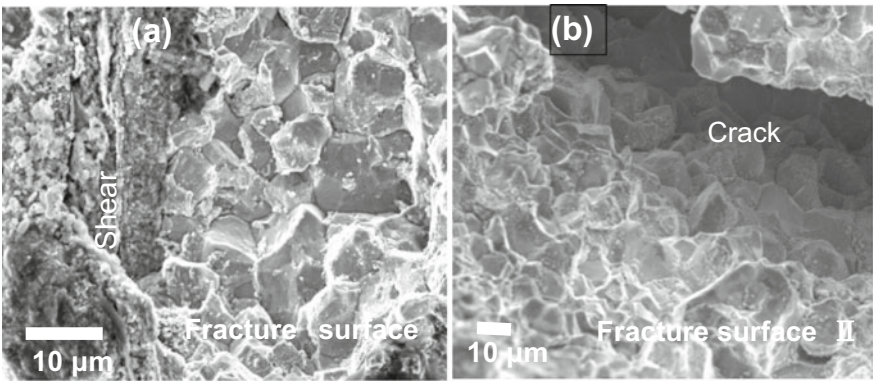

Fig. 11.12 **(a)** SEM micrograph of fracture surface I at the intersection with the outer surface of the bolt forming shear fracture. The area corresponds to the yellow dashed frame in Fig. 11.5(b). (**b)** SEM image of fracture surface II near and under crack opening 3 shown in Figs. 11.6 and 11.7. Both fracture surfaces I and II exhibit IG fracture (Homma et al. [5])

before macroscopic crack propagation, but the net-like cracking is consistent with the fractographic features. Figure 11.12(a), (b)[5] show the fracture surfaces I and II in Fig. 11.9. Both surfaces exhibit sharp IG fracture surfaces, and the 3-dimensional morphologies are coincident with Fig. 11.10. Some tiny particles, likely corrosion products, are present in Fig. 11.12(a), but sharp morphologies imply that heavy corrosion is not present.

IG fracture is usually regarded as a typical type of tensile stress-controlled brittle fracture. Local stress states are complicated in the presence of multiple cracks and stress relief upon the crack nucleation. However, IG fracture mode was dominant over a zone of about 500 μm in width, including sites close to the outer surface, as Figs. 11.7 and 11.9 exhibited. A specific stress or strain state is not definite to control the crack nucleation in the zone, while the fracture mode is IG. Figure 11.10 implied that the crack nucleation is neither stress- nor strain-controlled. IG fracture was present along a plane steeply inclined to the maximum tensile stress plane in the region where fracture surfaces I and II merged before the start of a macroscopic crack propagation, circle 5 in Fig. 11.7. The externally applied tensile stress is not the dominant cause of inducing IG fracture. In this aspect, insert (b) in Fig. 11.10 is indicative of the involvement of plasticity in IG fracture in hydrogen-charged martensitic steel, similar to Fig. 7.8.

Multiple nucleation of microcracks suggests damage accumulation preferentially along grain boundaries, ready to nucleate cracks there. The region beneath the screw groove is highly stressed, exceeding the elastic limit. Discontinuities in the crystalline orientations are preferential stress-intensification sites, and prior austenite grain boundaries act as barriers to slip extension or dislocation emission sites. Deterioration of areas neighboring the boundaries is a natural consequence of the associated generation of lattice defects. In atmospheric exposure, no intentional increase is applied in the external stress, but environmental variations are viable to cause changes

in internal stress, specifically in stress-concentrated areas. Accordingly, accumulation of damage in the frail zone may be prominent along grain boundaries, thus providing the macroscopic crack path.

11.3.4 Crack Propagation

11.3.4.1 Affinity of Different Fracture Morphologies

The macroscopic crack propagation starts from the periphery of the frail zone, not from a point like a second-phase particle. Fracture morphologies changed continuously from IG in the frail zone to QC and fine dimples, concomitantly with the crack propagation, as shown in Fig. 11.13 [5]. The changes correspond to fan-like contrasts in Fig. 11.6(b), as schematically shown in Fig. 11.14. A matter to consider is the reason for the changes or the affinity of different fracture morphologies.

QC and dimple fractures are plasticity-dominated, and some plasticity is also involved in IG fracture. The fracture morphology termed IG-like by Shibata et al., as an intermediate between IG and QC, suggests the involvement of plasticity in the

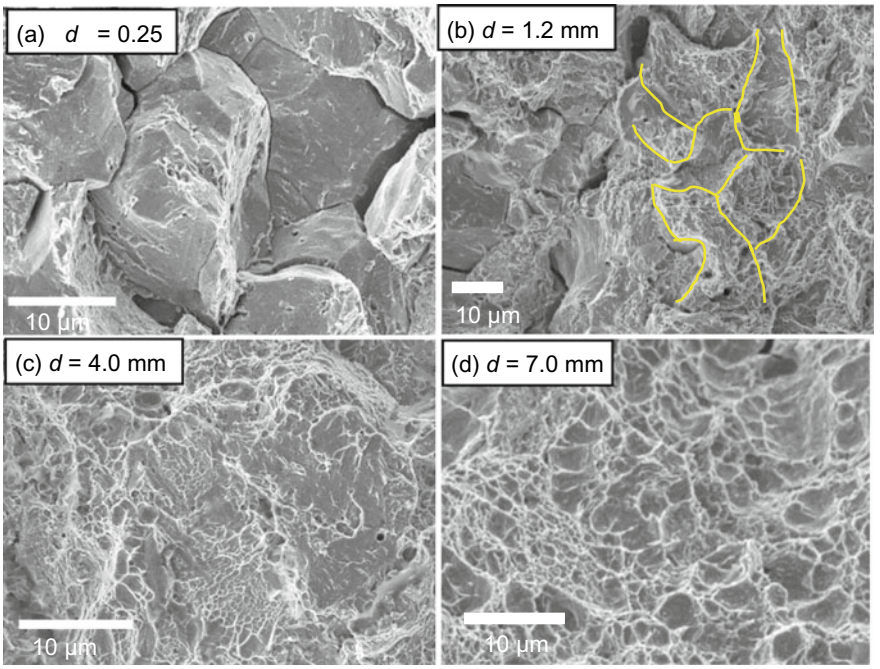

Fig. 11.13 Fractographic features associated with the crack advance. Panels (**a**)–(**d**) show fracture surfaces each at the indicated distance *d* from the edge of the fracture surface as marked in Fig. 11.5(b). Yellow lines in (**b**) are estimated prior austenite grain boundaries (Homma et al. [5])

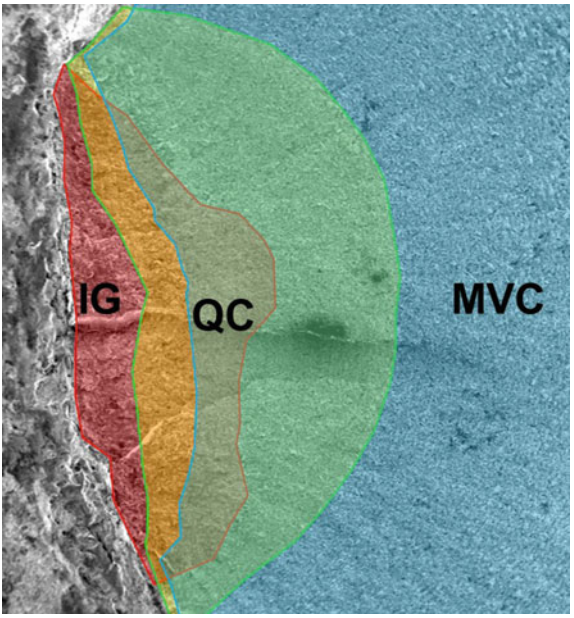

Fig. 11.14 Transition of the fracture morphologies with the crack propagation, corresponding to contrasts in Fig. 11.6(b)

close vicinity, of the order of 100 nm, of prior austenite grain boundaries [10]. In the present case, the IG surfaces in the frail zone, more or less associated with fine tear ridges (Fig. 11.13a), are worthy of the term IG-like. A branched crack along the grain boundary in the inset (b) in Fig. 11.10, showing the mating of flat and irregularly shaped surfaces, suggests a common origin for IG and IG-like.

Alteration of fracture morphology concomitant with crack growth was first observed and related to a decreasing stress intensity factor K by Beachem using a wedge-loading compact tension specimen [11], as described in Sect. 7.2.5. In the present case, the distance between the bolt head and the nut was fixed by the thickness of the fastened steel plate and two washers. The axial force is the product of the elastic stress and the cross-sectional area of the shank. In the crack propagation stage, the decrease in the cross-sectional area reduces the axial force. Still, the elastic displacement in the ligament is kept constant, implying that the applied elastic stress is unaltered except in the crack front region where the stress intensification operates. K is proportional to the square root of the crack length and increases with the crack growth. Quantitative estimation of K in the present case is difficult, but the qualitative K-dependence of fracture morphologies from IG to QC and fine dimples was consistent with the literature. Beachem did not mention the origin of the K-dependence, but increasing K would reasonably enlarge the highly stressed region in the crack front and activate dislocations therein, thus increasing the sites available for crack nucleation.

The alteration of fracture morphologies is moderate or gradual, such as blunting of sharp prior austenite grain shapes (Fig. 11.12b), broadening of boundaries between

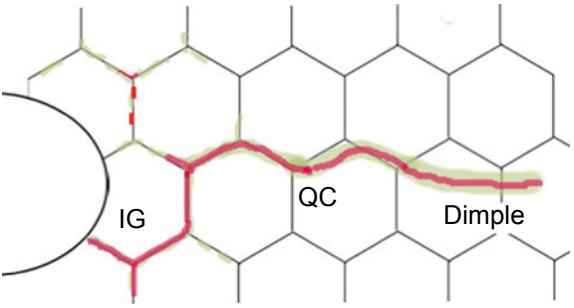

Fig. 11.15 Schematic illustration of the alteration of the crack propagation path from IG mode to QC mode and dimples as the crack propagates from the bottom of the screw thread. The crack and the associated damage zone are shown in red and green, respectively (Homma et al. [5])

IG and QC (Fig. 11.12b), and between QC and fine dimple surfaces (Fig. 11.12c, d). The potential crack path incorporates inhomogeneous sites accumulated of hydrogen and damage. A preferential crack path will initially be along prior austenite grain boundaries, retaining a three-dimensional configuration of grains. Associated with the crack extension, the enlargement of the highly stressed region in front of the propagating crack activates potential crack nucleation sites, increasing the density of nucleated cracks on a broader area.

A presumable crack growth process is as follows. The link of microcracks on grain boundaries is surely the early stage of macroscopic crack nucleation. Sharp boundary lines may appear when the extending crack meets another one and links with it. The plastic zone in front of a crack, expanding with the crack growth, blunts the meeting boundary lines but still keeps boundary shapes on the fracture surface. In the early stage of crack growth, the distribution of potential cack nucleation sites may determine the crack path along prior austenite grain boundaries. Further crack growth, however, enlarges the plastic zone and intensifies stress states therein. Potential crack nucleation sites then increase, and the applied stress, rather than the distribution of the sites, will be the primary factor to determine the crack path. Observed changes of fractographic features, Fig. 11.13, are consistent with the notion that strain-induced damage served as the common crack path. Different appearances of IG, IG-like, and QC might result from the extent of activate void nucleation sites in the crack path.

Figure 11.15 [5] schematically illustrates the alteration of the crack path associated with increasing K, omitting proper length scales and locations from the notch root. The driving force for the crack extension is the increasing K associated with the crack extension. The crack extension with small plasticity in the crack front, presented by Rice [14] and Rice-Wang [15] in Sects. 9.4.1 and 9.4.2, is viable. Deterioration of the crack front induced by diffusion of internal hydrogen is presented in the following section.

11.3.4.2 Step-Wise Crack Propagation

The initiation of the propagating crack was close to the outer surface of the bolt. A long-time atmospheric exposure likely deteriorated that part, but environmental

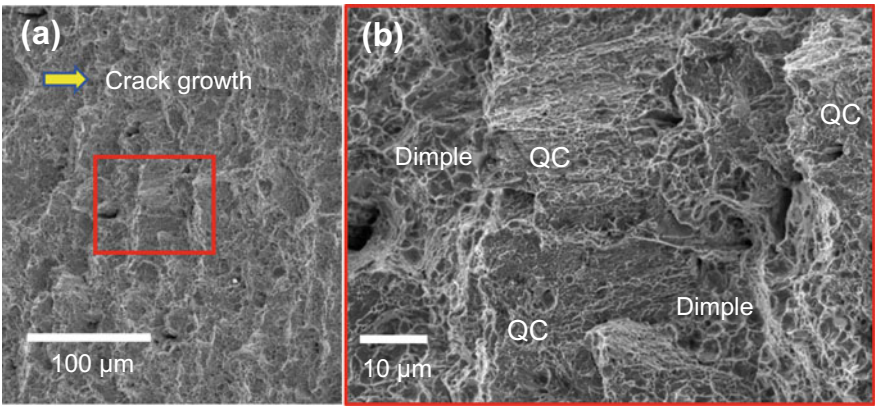

Fig. 11.16 **(a)** Striations perpendicular to the crack growth direction at a site about 8 mm from the edge. The specimen stage was tilted by 45° to the crack growth direction in order to enhance the contrast. **(b)** Magnified view of the red-framed area in (**a**) (Homma et al. [5])

effects, including the entry of hydrogen, must also affect the internal part of the bolt. Another issue is the pertinence of laboratory tests in evaluating delayed fracture. In this aspect, periodical striations perpendicular to the crack growth direction, shown in Fig. 11.16(a) [5], are noticed on the fracture surface propagating with QC morphology.

The hydrogen concentration after long-time atmospheric exposure would be reasonably uniform in the region outside the stress-concentrated frail zone at a value lower than that in the zone. When a crack propagates from the frail zone, stress intensification at the crack front will raise the hydrogen concentration therein. In this case, an external hydrogen supply from the atmosphere through a thin gap formed by the crack is hardly feasible. Internal diffusion, instead, would be the viable supply process. The observed striations would result from the periodic crack start and stop, associated with a repeated buildup of local hydrogen concentration to the critical level. In a laboratory test using hydrogen-precharged specimens, Wang et al. calculated the buildup of the hydrogen concentration at the notch root using a stress-driven hydrogen diffusion equation [12], as described in Sect. 6.4.4b. The time required to reach a steady state was a few hundred minutes for their experimental condition. On the other hand, in the propagating sharp crack, the crack advance is expected to occur at a hydrogen concentration of a certain level, likely in the frail zone, before reaching the steady-state value. The local hydrogen concentration is an exponential function of triaxial stress. According to the calculated stress concentration for the circumferentially notched round bar in Fig. 11.3 or the screw-threaded bolt [13], the estimated maximum hydrogen concentration in the vicinity of the screw groove was not so high, likely 1.5–1.8 times the average value C_0 in the bolt.

An exact quantitative estimation is difficult, but the time spent raising the crack front hydrogen concentration to a critical level would be much shorter than a few hundred minutes to reach steady states (3 ~ 4 C_0) in the notch root in Wang's case

[12]. In the present case, the slightly rusting fracture surface shown in Fig. 11.5 suggested that the crack propagated for about one week. Then, the observed width of about 50 μm between striations (Fig. 11.16) gave about 20 min for a one-step crack advance when assumed that the crack propagated 10 mm in three days. The estimated crack growth rate conforms roughly to the order of magnitude with the calculated time for the buildup of hydrogen concentration using Wang's results [12].

The crack propagation process outside the frail zone may be similar to that in the laboratory constant load delayed fracture test [12], where hydrogen supply to the critical site is decisive for cracking. Hydrogen supply will stimulate dislocation dynamics and generate additional damage to start cracking at sites where densities of dislocations and vacancies are already substantial. However, a steep hydrogen concentration gradient would deprive the restarted crack of the driving force after a short advance under a constant-displacement condition. The situations of laboratory tests of delayed fracture under constant load using hydrogen-enclosed notched specimens may correspond to the step-wise crack propagation stage in the present case. Acoustic emission waveforms originating in either plasticity or cracking, shown in Fig. 6.26 during a laboratory sustained-loading test of round bar specimens, may correspond to the crack precursory and step-wise crack propagation, respectively, in the present atmospheric exposure.

11.4 Assessment of the Susceptibility to Delayed Fracture

Assessment of the safety of structural components against delayed fracture is a crucial subject in engineering service. Some methods have been proposed to "evaluate" the resistance to delayed fracture of high-strength steel [13, 16], assuming that the critical hydrogen concentration H_C determines the onset of delayed fracture, as described in Sects. 6.4.4 and 6.4.5. The proposed "evaluation" methods are *laboratory procedures to determine* H_C, and an estimation of environmental effects is additionally necessary for assessing the performance in atmospheric exposure. However, environments that structural components tolerate during service are diverse, and an exact simulation is difficult.

The term "evaluation" in the proposed methods means a "quantitative characterization" of delayed fracture, neither "qualification" nor "assessment" of the performance of steel. Reliable methods to assess the safety or performance of steel in long-time atmospheric exposure have not been present for use. However, as described in the preceding chapters, recent advances are substantial in understanding the characteristics of HE of steel and materials' response to hydrogen. A noteworthy finding is that hydrogen per se is not the decisive player in the embrittlement, without any evidence of H_C in failure at long-time atmospheric exposure. When the hydrogen concentration is no longer viable as the measure, an alternative approach to assessing the susceptibility to delayed fracture of steel is to be addressed to interactions of hydrogen and lattice defects that directly operate in fracture.

Materials and external factors affecting delayed fracture are described in Sects. 6.4.2 and 6.4.3, and the involvement of strain-induced vacancies in HE is briefly summarized in Sect. 10.5.1. Hydrogen degradation manifests under various types of loading, and generated damage of materials in various loading is versatile in causing degradation. The common function of hydrogen in enhancing vacancy generation implies the feasibility of a parameter that represents the intrinsic susceptibility of materials to HE. In this respect, noteworthy findings are the effects of environmental variations on sustained-loading delayed fracture in Sect. 6.4.3 and the carry-over of damage produced in the early stages of deformation to the final fracture stage in Sect. 7.4.2.

In atmospheric exposure, environmental variations are viable factors that induce microstructural alteration and generate damage that accumulates during service. Nagumo and Takai proposed a method to assess steel's intrinsic susceptibility to HE [17]. A remarked finding as a background was laboratory results that demonstrated cyclic variations of the applied stress to promote failure in sustained-loading tests of high-strength steel despite a decrease in the average applied-stress level, Fig. 6.30. Similarly, cyclic variations of hydrogen-charging current densities promoted failure while the introduced hydrogen contents were the same, Fig. 6.31. Thermal desorption analysis (TDA) of hydrogen introduced as the tracer of defects exhibited the generation of vacancy-type defects during the incubation period.

A precise experiment for the effects of cyclic prestressing on tensile tests of high-strength steel is shown in Fig. 7.23. The cyclic prestressing under hydrogen charging reduced the tensile-fracture strain, more prominently by decreasing the strain rate at the prestressing. The cyclic prestressing generates vacancy-type defects that deteriorate the following tensile properties, and its extent under a given condition may depend on steel. As a parameter to express the effects of cyclic prestressing on deterioration, the hydrogen-enhanced increase in lattice defects was denoted as ΔC_H [18]. ΔC_H is defined as the difference of the amount of tracer-hydrogen between specimens subjected to cyclic stressing with and without hydrogen. ΔC_H increases with the number of cyclic stressing and is higher with lower strain rates, as shown in Fig. 7.24, well-characterizing features of HE.

ΔC_H represents the intrinsic stability of microstructures against external excitement in the presence of hydrogen. The proposal by Nagumo and Takai was to use ΔC_H as a versatile parameter for assessing the susceptibility of steel to HE, not limited to delayed fracture in atmospheric exposure. ΔC_H is a relative measure of the susceptibility among different types of steel, and a standard material is separately necessary for safety design in engineering practice. The correlation between the crack growth resistance and the amount of hydrogen as a tracer of lattice defects, shown in Figs. 10.4 and 10.5, implicates the versatility of the role of strain-induced vacancies in fracture events. The three low-carbon steels were characterized by different areas of slip constraint phases along grain boundaries, enhancing the local generation of lattice defects.

11.5 Concluding Remarks

Delayed fracture of high-strength steel in long-time atmospheric exposure is like alpha and omega for the hydrogen embrittlement problem of steel. Delayed fracture after long-time atmospheric exposure is peculiar among various fracture events regarding the driving force. Its entity has been left unclear because of the poor supply of proper materials. Reference [5] is the first report that detailed the cracking process in delayed fracture of high-strength steel bolts in engineering practice. Recent studies in laboratories have revealed characteristic features of HE with the aid of advanced tools. The enhanced generation of vacancies coupled with plasticity, the HESIV mechanism, and the damage accumulation and deterioration of materials are the viable and essential functions of hydrogen, deduced from recent studies on diverse manifestations of HE. The cracking process revealed in Ref. [5] conforms with this notion. Inversely, the present results testify to the idea about the function of hydrogen deduced from laboratory tests. However, further studies must enrich the present limited observations and reveal more details.

Assessment of materials' safety or performance is crucial for engineering practice, but conventional methods are mostly empirical judgments. A reason is the difficulty in correctly simulating engineering use, and an alternative approach based on reliable principles is inevitable. The proposed method [17] might be versatile in diverse manifestations of HE, standing on presumed essential functions of hydrogen rather than specific empirical data. To test the proposal in practical service is a future subject. A wide scatter of the time to failure extending over years is another matter for future studies, likely a problem of the stochastic process.

References

1. Japanese Industrial Standard JISB1186–1995, Sets of high strength hexagonal bolt, hexagon nut and plain washers for friction grip joints (1995)
2. N.J. Petch, Phil. Mag. **1**, 331–337 (1956)
3. M. Yamaguchi, J. Kameda, K. Ebihara, M. Itakura, H. Kaburaki, Phil. Mag. **92**, 1349–1368 (2012)
4. S. Li, E. Akiyama, N. Uno, K. Hirai, K. Tsuzaki, B. Zhang, Corros. Sci. **52**, 3198–3204 (2010)
5. T. Homma, T. Chiba, K. Takai, E. Akiyama, W. Oshikawa, M. Nagumo, ISIJ Int. **62**, 776–787 (2022)
6. T. Kobayashi, D.A. Shockey, Metall. Trans. A **18A**, 1941–1949 (1987)
7. S. Yamazaki, T. Takahashi, T. Kobayashi, Tetsu-to-Hagané **83**, 526–531 (1997)
8. A. Shibata, Y. Momotani, T. Murata, T. Matsuoka, M. Tsuboi, N. Tsuji, Mater. Sci. Tech. **33**, 1524–1532 (2017)
9. Y. Ding, H. Yu, M. Lin, K. Zhao, S. Xiao, A. Vinogradov, L. Qiao, M. Ortiz, J. He, Z. Zhang, Acta Mater. **239**, 118279 (2022)
10. A. Shibata, T. Murata, H. Takahashi, T. Matsuoka, N. Tsuji, Metall. Mater. Trans. A **46A**, 5685–5696 (2015)
11. C.D. Beachem, Metall. Trans. **3**, 437–451 (1972)
12. J.R. Rice: in *Proceedings of International Conference Fracture*, vol. 1. The Japan Society for Promotion of Science, pp. A269-A318 (1965)

13. J.R. Rice, J.-S Wang, Mater. Sci. Eng. **A107**(1989), 23–40
14. M. Wang, E. Akiyama, K. Tsuzaki, Corros. Sci. **48**, 2189–2202 (2006)
15. Guidebook for evaluation of delayed fracture property of high strength bolts, JSSC Technical Report #91, Japanese Society of Steel Construction, Tokyo (2010), Chap. 4 (in Japanese)
16. International Organization for Standardization (ISO), Measurement method for the evaluation of hydrogen embrittlement resistance of high strength steels, ISO 16573 (2015)
17. M. Nagumo, K. Takai, Mater. Sci. Tech. **36**, 1003–1011 (2020)
18. T. Doshida, M. Nakamura, H. Saito, T. Sawada, K. Takai, Acta Mater. **61**, 7755–7766 (2013)